JOURNAL OF SPACECRAFT AND ROCKETS
Vol. 42, No. 1, January–February 2005

Flat-Faced Leading-Edge Effects in Low-Density Hypersonic Wedge Flow

Wilson F. N. Santos[*]
National Institute for Space Research, SP 12630-000 Cachoeira Paulista, Brazil

A numerical study was performed to determine the upstream effects of leading-edge thickness on the rarefied hypersonic flow over truncated wedges at zero angle of attack. The simulations were performed by using the direct simulation Monte Carlo (DSMC) method. A method that has demonstrated excellent comparisons with flight- and ground-test data, it properly accounts for nonequilibrium aspects of the flow that arise near the leading edge, which are especially important at high Mach numbers. Some significant differences between sharp and blunt leading edges were noted on the flowfield structure and on the aerodynamic surface quantities. It was found that the upstream effects have a different influence on the stagnation streamline properties ahead of the leading edges depending on the leading-edge Knudsen number. Interesting features observed in the surface fluxes showed that small leading-edge thickness, compared to the freestream mean free path, has important effects on high-Mach-number leading-edge flows. Also, effects on the skin-friction coefficient, pressure coefficient, and heat-transfer coefficient on the wedge are presented as a function of thickness Knudsen number.

Nomenclature

a = speed of sound, m/s
C_d = drag coefficient, $2F/\rho_\infty V_\infty^2 H$
C_f = skin-friction coefficient, $2\tau_w/\rho_\infty V_\infty^2$
C_h = heat-transfer coefficient, $2q_w/\rho_\infty V_\infty^3$
C_p = pressure coefficient, $2(p_w - p_\infty)/\rho_\infty V_\infty^2$
F = drag force, N
H = body height at the base, m
Kn = Knudsen number, λ/l
L = body length, m
l = characteristic length, m
M = Mach number, V/a
N = number flux, $\mathrm{m}^{-2}\mathrm{s}^{-1}$
n = number density, m^{-3}
p = pressure, $\mathrm{N/m}^2$
q = heat flux, $\mathrm{W/m}^2$
R = circular cylinder radius, m
Re = Reynolds number, $\rho V l/\mu$
St = Stanton number, $h/\rho c_p V$
s = arc length, m
T = temperature, K
t = leading-edge thickness, m
V = velocity, m/s
x, y = Cartesian axes in physical space, m
γ = ratio of specific heats
η = coordinate normal to body surface, m
θ = wedge half-angle, deg
λ = mean free path, m
ξ = coordinate tangent to body surface, m
ρ = density, $\mathrm{kg/m}^3$
τ = shear stress, $\mathrm{N/m}^2$

Subscripts

w = wall condition
0 = stagnation condition
∞ = freestream condition, infinity
$*$ = reference state

Introduction

HYPERSONIC configurations are generally characterized by slender bodies and sharp leading edges in order to achieve good aerodynamic properties like high lift and low drag. Certain configurations, such as waveriders,[1] are designed analytically with infinity sharp leading edges for shock-wave attachment. Because the shock wave is attached to the leading edge of the vehicle, the upper and lower surfaces of the vehicle can be designed separately. Moreover, the shock wave can prevent spillage of higher-pressure airflow from the lower side of the vehicle to the upper side, resulting in a high-pressure differential and enhanced lift.

Usually, it is extremely difficult to construct a perfectly sharp leading edge. Any manufacturing error results in a significant deviation from the design contour. Furthermore, sharp edges are difficult to maintain because they are easily damaged. Additionally, because heat transfer increases inversely with the leading-edge radius high heating is associated with sharp edges. Therefore, for practical hypersonic configurations leading edges are blunted for heat transfer, manufacturing, and handling concerns. Because blunt leading edge promotes shock standoff, practical leading edges will have shock detachment, making leading-edge blunting a major concern in the design and prediction of flowfields over hypersonic configurations.

Experimental and theoretical works on hypersonic flow past wedges have been concentrated primarily on the analysis of the flowfield by considering the leading edges as being aerodynamically sharp. A critical study providing information on maximum allowable edge thickness for a given flow pattern has not received considerable attention. Such information is important when a comparison is to be made between experimental results in the immediate vicinity of the leading edge and the theoretical results, which generally assume a zero-thickness leading edge.

There has been a rather limited investigation of the flowfield associated with wedges under hypersonic flow. Cheng et al.[2] presented results of a theoretical and experimental study of leading-edge bluntness and boundary-layer displacement effects in hypersonic flow over thin bodies. Their theoretical solution was developed based on a continuum flow model in the strong interaction region. Experimental heat-transfer and pressure data obtained with two-dimensional wedge models were presented by Vidal and Bartz.[3] The purpose of their investigation was to test the available theories dealing with wedges in a continuum flow in order to define their limits of validity

---

Received 1 September 2003; revision received 3 December 2003; accepted for publication 3 December 2003. Copyright © 2003 by the Instituto Nacional de Pesquisas Espaciais. Published by the American Institute of Aeronautics and Astronautics, Inc., with permission. Copies of this paper may be made for personal or internal use, on condition that the copier pay the $10.00 per-copy fee to the Copyright Clearance Center, Inc., 222 Rosewood Drive, Danvers, MA 01923; include the code 0022-4650/05 $10.00 in correspondence with the CCC.

[*] Researcher, Combustion and Propulsion Laboratory. Member AIAA.

and to provide data in the transition regime, that is, between the conventional continuum flow and the free-molecular flow. Their comparison was restricted to the boundary-layer theory and the viscous shock-layer theory.

McCroskey et al.[4] investigated experimentally the hypersonic flow on plates, wedges, and cones. Pressure and density profiles adjacent to the bodies as well as the shock-wave shapes were presented downstream of the leading edges. The results were restricted to the merged-layer region, where the shock layer begins to thicken and merges with the boundary layer. Vidal and Bartz[5] performed a series of low-density experiments with a flat plate at small (2–10 deg) and large wedge angles (20–40 deg). The purpose of their study was twofold: 1) to investigate the viscous shock-layer regime under the combined effects of boundary-layer displacement and wedge angle for plates at small wedge angles and 2) to investigate the viscous shock-layer regime under conditions where the boundary-layer displacement effects should be negligible, for plates at large wedge angles. The results included direct measurements of surface pressure, skin friction, and heat transfer, which were used to infer the jump conditions at the surface.

Allgre et al.[6] conducted measurements of surface pressure, drag, and lift on flat plates and wedges for different values of incidence and leading-edge bluntness in a hypersonic flow. The purpose of their investigation was to study the bluntness effect on boundary-layer displacement thickness in the hypersonic interaction regime. In this regime, located far downstream of the leading edge, the flow behaves like an ordinary viscous flow with a Prandtl-type boundary layer near the body surface.

Finally, Klemm and Giddens[7] obtained a solution for the flowfield on a finite-length sharp wedge immersed in a low-density flow. Their results, obtained by employing the Boltzmann equation with the Bhatnagar, Gross, and Krook (BGK) collision model, illustrated the extent of the upstream influence on the macroscopic properties that included the number density and temperature and the complex nature of the flow in the wake region.

The flowfield properties upstream of the leading edge of a body are affected by molecules reflected from the edge region. The degree of the effect is in part conditioned by the edge geometry. In this context, the purpose of this paper is to investigate the effect of the leading-edge thickness, hence the Kn_t on the flowfield structure and on the aerodynamic surface quantities over truncated wedges. By considering the recent interest on hypersonic waveriders for high-altitude/low-density applications,[8–11] the Kn_t effects will be investigated from the transition regime to the free molecular flow.

For the transitional hypersonic flow at high Mach number and high altitude, the flow departs from thermal equilibrium and the energy exchange into the various modes as a result of the vibrational excitation, and relaxation becomes important. In this scenario, the degree of molecular nonequilibrium is such that the Navier–Stokes equations are inappropriate. Alternatively, the direct simulation Monte Carlo (DSMC) method is used in the current study to simulate the rarefied hypersonic two-dimensional flow.

Leading-Edge Geometry Definition

The truncated wedges analyzed in this work are modeled by assuming a sharp leading edge of half-angle θ with a circular cylinder of radius R inscribed tangent to this sharp leading edge. The truncated wedges are also tangent to the sharp leading edge and the cylinder. It assumed a leading-edge half-angle of 10 deg, a circular cylinder diameter of 10^{-2} m, and truncated wedge thicknesses t/λ_∞ of 0.0, 0.01, 0.1, and 1.0, where λ_∞ is the freestream mean free path with corresponding Kn_t of ∞, 100, 10, and 1, respectively. Figure 1 illustrates schematically this construction. The common body height H and the body length L are obtained in a straightforward manner. This construction produces a flat leading edge.

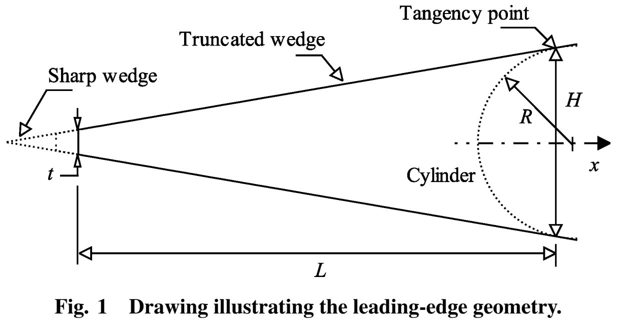

Fig. 1 Drawing illustrating the leading-edge geometry.

Computational Method and Procedure

A number of significant problems in fluid mechanics involve transitional flows, that is, flows for which the mean free path is of the same order of magnitude as a characteristic dimension of the problem. The most successful numerical technique for modeling complex transitional flows has been the DSMC method, pioneered by Bird.[12] The DSMC method has become one of the standard numerical techniques for modeling complex flows in the regimes where neither the Navier–Stokes nor the free molecular approaches are appropriate.

The DSMC method models the flow as being a collection of representative particles, each one with a position, velocity, and internal energy. The particles are tracked as they move, collide, and undergo boundary interactions in simulated physical space. Each simulated particle represents a much larger number of real particles. The molecular motion, which is considered to be deterministic, and the intermolecular collisions, which are considered to be stochastic, are uncoupled over the small time step used to advance the simulation and computed sequentially. In general, the step ought to be sufficiently small in comparison with the local mean collision time.[13]

In this study, the molecular collisions are modeled using the variable-hard-sphere (VHS) molecular model.[14] This model employs the simple hard-sphere angular scattering law so that all directions are equally possible for postcollision velocity in the center-of-mass frame of reference. However, the collision cross section depends on the relative speed of colliding molecules. The energy exchange between kinetic and internal modes is controlled by the Borgnakke–Larsen statistical model.[15] The essential feature of this model is that a part of collisions is treated as completely inelastic, and the remainder of the molecular collisions is regarded as elastic. Simulations are performed using a nonreacting gas model consisting of two chemical species, N_2 and O_2. The probability of an inelastic collision determines the rate at which energy is transferred between the translational and internal modes after an inelastic collision. For a given collision, the probabilities are designated by the inverse of the relaxation numbers, which correspond to the number of collisions necessary, on average, for a molecule to relax. The relaxation numbers are traditionally given as constants, 5 for rotation and 50 for vibration.

The physical space is divided into a number of regions, which are subdivided into computational cells. The cells are further subdivided into four subcells, two subcells in each coordinate direction. The cell provides a convenient reference for the sampling of the macroscopic gas properties, whereas the collision partners are selected from the same subcell for the establishment of the collision rate. Consequently, the flow resolution is much higher than the cell resolution. The dimensions of the cells must be such that the change in flow properties across each cell is small. The linear dimensions of the cells should be small in comparison with the scale length of the macroscopic flow gradients in the streamwise directions, which means that the cell dimensions should be of the order of the local mean free path or even smaller.[16–18]

In simulating rarefied flows, the computational flow domain must extent far enough upstream of the body in order to provide ample opportunity for freestream molecules to interact with those molecules that have reflected from the body and are diffusing into the flow. Insufficient upstream domain size leads to overprediction of aerodynamic heating and forces.[19] In this context, the computational domain, shown in Fig. 2, is made large enough so that the upstream and side boundaries can be specified as freestream conditions. The flow at the downstream outflow boundary is supersonic, and vacuum conditions are specified.[12] At this boundary, simulated molecules can

Table 1 Freestream flow conditions

Parameter	Value
Temperature T_∞	220.0 K
Pressure p_∞	5.582 N/m^2
Density ρ_∞	8.753×10^{-5} kg/m^3
Viscosity μ_∞	1.455×10^{-5} Ns/m^2
Number density n_∞	1.8209×10^{21} m^{-3}
Mean free path λ_∞	9.03×10^{-4} m

Table 2 Gas properties

Parameter	O_2	N_2
Molecular mass	5.312×10^{-26} kg	4.65×10^{-26} kg
Molecular diameter	4.010×10^{-10} m	4.11×10^{-10} m
Mole fraction	0.237	0.763
Viscosity index	0.77	0.74

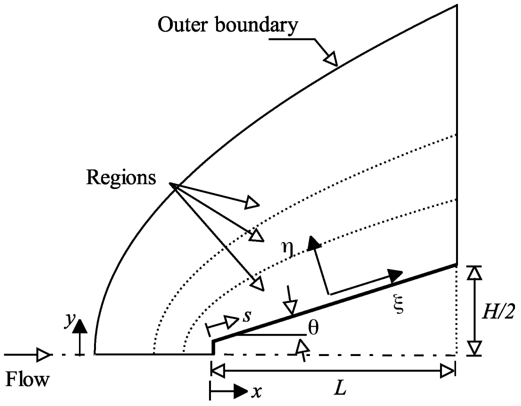

Fig. 2 Schematic view of the computational domain.

only exit. Diffuse reflection with complete thermal accommodation is the condition applied to the body surface. Advantage of flow symmetry is taken into account, and molecular simulation is applied to one-half of a full configuration in order to reduce the computational domain.

Numerical accuracy in DSMC method depends on the grid resolution chosen as well as the number of particles per computational cell.[19] Both effects were investigated to determine the number of cells and the number of particles required to achieve grid-independence solutions for the thermal nonequilibrium flow that arises near the nose of the leading edges.

A grid-independence study was made with three different structured meshes in each direction. The effect of altering the cell size in the ξ direction was investigated with grids of 50 (coarse), 100 (standard), and 150 (fine) cells, and 60 cells in the η direction. In analogous fashion, an examination was made in the η direction with grids of 30 (coarse), 60 (standard), and 90 (fine) cells and 100 cells in the ξ direction. Each grid was made up of nonuniform cell spacing in both directions. The effect (not shown) of changing the cell size in both directions on the heat transfer, pressure, and skin-friction coefficients was rather insensitive to the range of cell spacing considered, indicating that the standard grid, 100×60 cells, is essentially grid independent.

A similar examination was made for the number of molecules. The standard grid, 100×60 cells, corresponds to, on average, a total of 190,000 molecules. Two new cases using the same grid, corresponding to 104,000 and 283,000 molecules in the entire computational domain, were investigated. As the three cases presented approximately the same results (not shown) for the heat transfer, pressure, and skin-friction coefficients, then the standard grid with a total of 190,000 molecules is enough for the computation of the aerodynamic surface quantities.

The freestream and flow conditions used in the present calculations represent those experienced by a flight vehicle at an altitude of 70 km. Tables 1 and 2 summarize the freestream conditions[20] and the gas properties,[12] respectively. The freestream velocity V_∞ is assumed to be constant at 3.56 km/s, which corresponds to freestream Mach number M_∞ of 12. The wall temperature T_w is assumed constant at 880 K.

The overall Knudsen number Kn is defined as the ratio of the molecular mean free path λ in the freestream gas to a characteristic dimension of the flowfield. Hence, the characteristic dimension was defined as being the thickness t of the truncated leading edges. For the thicknesses investigated, $t/\lambda_\infty = 0$, 0.01, 0.1, and 1.0, the overall Knudsen numbers correspond to $Kn_t = \infty$, 100, 10, and 1, respectively. Note that for $Kn_t = \infty$ the leading edge is sharp. The Reynolds number Re_t covers the range from 0.193 to 19.3, based on conditions in the undisturbed stream with leading-edge thickness t as the characteristic length.

Computational Results and Discussion

Attention is now focused on the calculations of the flowfield properties and aerodynamic surface quantities obtained from DSMC. The flowfield properties of particular interest in the transition flow regime are velocity, density, pressure, and temperature, and the aerodynamic surface quantities of particular interest are number flux, pressure, heat transfer, skin friction, and drag. The purpose of this section is to discuss and to compare differences in the profiles of these properties caused by variations in the leading-edge thickness.

Flowfield Structure

The variations on the normal velocity profiles along the stagnation streamline caused by changes on the leading-edge thickness are illustrated in Fig. 3. In this figure, the normal velocity u is expressed as a fraction of the freestream velocity V_∞, and x/λ_∞ is the dimensionless distance upstream of the leading edge.

Figure 3 demonstrates that the leading-edge thickness influences the flowfield far upstream. This domain of influence increases with increasing the leading-edge thickness. This results from the upstream diffusion of particles that are reflected from the leading edge. Therefore, increasing the flat portion of the wedge (increasing t) leads to significantly larger disturbance upstream of the body. For instance, the upstream distance for a velocity reduction of 1% ($u/V_\infty = 0.99$) is around $1.6\lambda_\infty$, $1.8\lambda_\infty$, $2.4\lambda_\infty$, and $4.5\lambda_\infty$ for cases Kn_t of ∞, 100, 10, and 1, respectively.

Figure 4 displays the magnitude of the velocity slip u_w, normalized by the freestream velocity V_∞, along the afterbody surface of the wedge as a function of the dimensionless arc length s/λ_∞ measured from the shoulder of the wedge. It is seen that velocity slip presents the maximum value at the shoulder of the leading edges and decreases downstream along the wedge surface. As the leading-edge thickness increases, the velocity slip decreases. This indicates that the outer extent of the flowfield disturbance above the surface is much smaller for the sharp leading-edge case than that for blunt leading-edge cases. For the sharp leading-edge case, $Kn_t = \infty$, the maximum velocity slip is around 33% of the freestream velocity. In contrast, for the blunt leading-edge case, $Kn_t = 1.0$, the maximum velocity slip is only 15% of the freestream velocity.

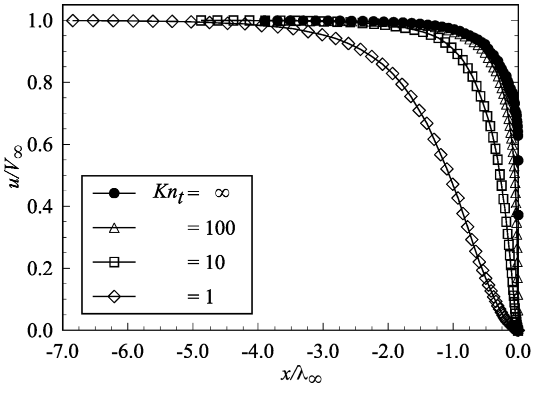

Fig. 3 Normal velocity profiles along the stagnation streamline as a function of the Knudsen number Kn_t.

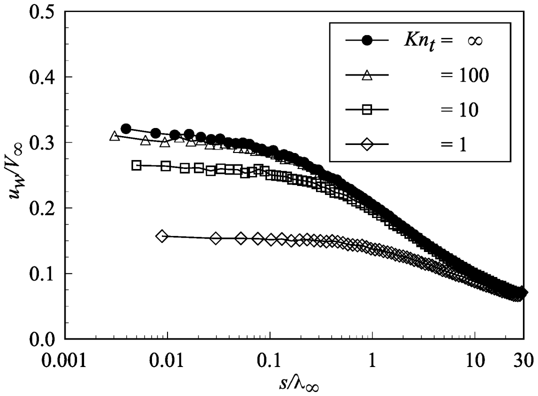

Fig. 4 Velocity slip profiles along the stagnation streamline as a function of the Knudsen number Kn_t.

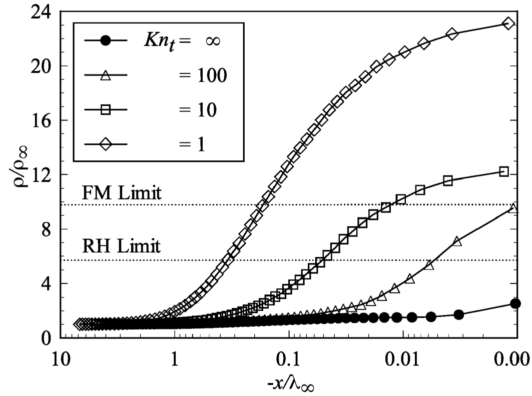

Fig. 5 Density profiles along the stagnation streamline as a function of the Knudsen number Kn_t.

It is observed from Figs. 3 and 4 that for the truncated wedge with thickness of one-hundredth of the freestream mean free path ($Kn_t = 100$) the normal velocity and the velocity slip are not strongly affected, as compared to the sharp wedge case ($Kn_t = \infty$).

Density profiles along the stagnation streamline are plotted as a function of the leading-edge thickness in Fig. 5. The predictions of density for all of the leading-edge thicknesses investigated show no sign of a discrete shock wave. Instead, there is a continuous rise in density from the freestream to the nose of the wedge, rising to well above the continuum inviscid limit. For comparison purposes, the Rankine–Hugoniot (RH) relations give a postshock density that corresponds to the ratio $\rho/\rho_\infty = 5.8$ for freestream Mach number of 12 (see Fig. 5). Near the stagnation point ($-x/\lambda_\infty = 0$), a substantial density increase occurs, which is a characteristic of cold-wall entry flow.[19]

It can be observed from these profiles that density rises gradually as the flow approaches the flat nose of the wedge, indicating the diffuse nature of the shock wave, a characteristic of highly rarefied flows. As the leading edge becomes flatter (t increases), the extent of the flowfield disturbances becomes much larger, as evidenced by the density profiles. Much of the density increase in the shock layer occurs after the temperature has reached its postshock value, as will be shown subsequently.

For the flow conditions investigated, the free molecular flow equations[12] predict a density ratio of 9.89 (see Fig. 5) at the stagnation point for the truncated wedges. As can be seen, the density ratio for the $Kn_t = 100$ case is approaching the free-molecular (FM) value at the stagnation point.

Pressure profiles along the stagnation streamline are shown in Fig. 6 as a function of the Kn_t. In this figure, pressure is normalized by the freestream pressure p_∞. As can be noted, similarly to density, there is a continuous rise in pressure from the freestream up to the nose of the leading edge. Near the stagnation point, a substantial pressure increase occurs. This pressure increase is a function of the leading-edge thickness t. It is also observed that the extent of the upstream flowfield disturbance for pressure is significantly different from those presented by density.

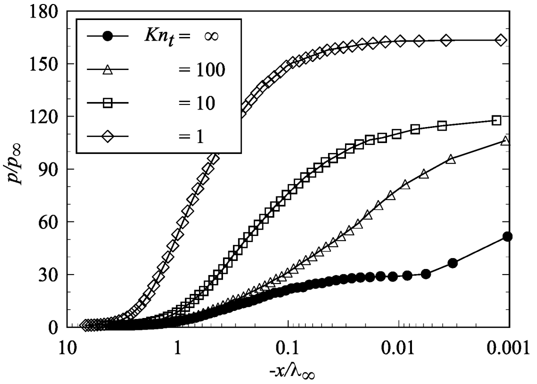

Fig. 6 Pressure profiles along the stagnation streamline as a function of the Knudsen number Kn_t.

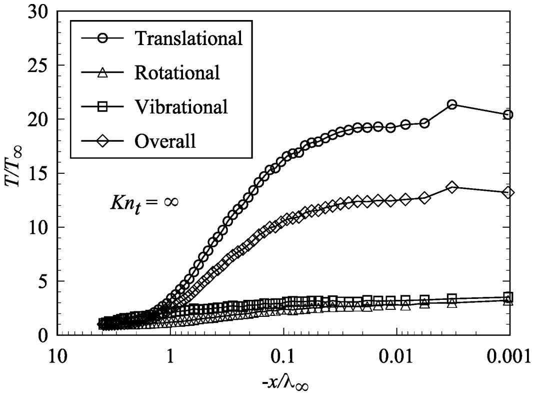

a) $Kn_t = \infty$ case

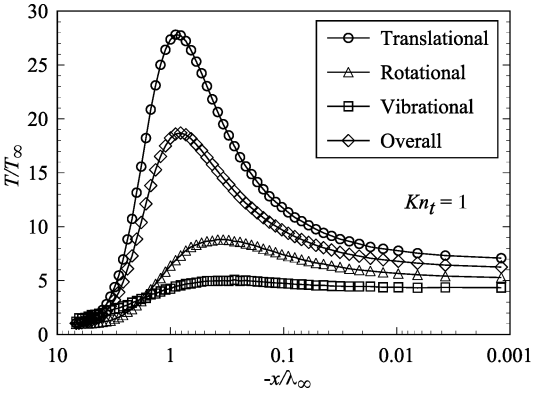

b) $Kn_t = 1$ case

Fig. 7 Kinetic temperature profiles along the stagnation streamline as a function of the Knudsen number Kn_t.

Figure 7 shows the kinetic temperature profiles, normalized by the freestream temperature T_∞, along the stagnation streamline for dimensionless leading-edge thicknesses of 0.0 and 1.0, Kn_t of ∞ and 1, respectively. According to Fig. 7, thermodynamic nonequilibrium is observed throughout the shock layer, as shown by the lack of equilibrium of the translational and internal kinetic temperatures. Thermal nonequilibrium occurs when the temperatures associated with the translational, rotational, and vibrational modes of a polyatomic gas are different. The overall kinetic temperature shown is defined for a nonequilibrium gas as the weighted mean of the translational and internal temperature.[12]

Referring to Fig. 7, in the undisturbed freestream far from the body, the translational and internal temperatures have the same value and are equal to the thermodynamic temperature. Approaching the nose of the leading edge, the translational temperature rises to well above the rotational and vibrational temperatures and reaches a maximum value that is a function of the leading-edge thickness. Because a larger number of collisions are needed to excite molecules vibrationally from the ground state to the upper state, the vibrational temperature increases much more slowly than rotational temperature. Still farther downstream toward the nose of the wedge, the translational temperature decreases for flat-faced leading edges and reaches a value on the wall that is above the wall temperature, resulting in a temperature jump as defined in a continuum formulation.[21]

The substantial rise in translational kinetic temperature for flat-faced leading edges occurred before the density rise (see Fig. 5). For instance, the kinetic translational temperature reaches the maximum value at a distance of one freestream mean free path from the nose of the leading edge for the $Kn_t = 1$ case, whereas the density ratio ρ/ρ_∞ is around 1.9 at the same station. The initial translational kinetic temperature rise for blunt leading edges results from the essentially bimodal velocity distribution[22]: the molecular sample consisting of mostly undisturbed freestream molecules with the molecules that have been affected by the shock and reflected from the body. In this way, the translational kinetic temperature rise is a consequence of the large velocity separation between these two classes of molecules.

Flattening the leading edge moves the shock wave created during the hypersonic flight forward and out, away from the leading edge. This shock wave that forms ahead of a blunt leading edge at hypersonic flow converts the kinetic energy of the freestream air molecules into thermal energy. This thermal energy downstream of the shock wave is partitioned into increasing the translational kinetic energy of the air molecules and into exciting other molecular energy states such as rotation and vibration (see Fig. 7). Most of the energy remains with the air molecules as they flow around the body. As a result, the heat flux to the body surface will be relatively low, as shown later.

Surface Quantities

The number flux N is calculated by sampling the molecules impinging on the surface by unit time and unit area. Results are normalized by $n_\infty V_\infty$, where n_∞ is the freestream number density and V_∞ is the freestream velocity. The sensitivity of the dimensionless number flux to variations on the leading-edge thickness is illustrated in Fig. 8. Figure 8a shows the dimensionless number flux to the front surface as a function of the dimensionless height y/λ_∞, measured from the stagnation point up to the shoulder of the wedge. The dimensionless number flux along the afterbody surface of the wedge is plotted in Fig. 8b as a function of the dimensionless arc length s/λ_∞, measured from the shoulder of the leading edge. Also, both plots present the free molecular flow limit for the dimensionless number flux by assuming free collision flow.[12]

It is seen from Fig. 8a that the dimensionless number flux is high near the stagnation point and decreases along the front surface up to the wedge shoulder as the thickness increases (Kn_t decreases). As the leading-edge thickness decreases (Kn_t increases), the dimensionless number flux to the front surface decreases and approaches the limit value ($N/n_\infty V_\infty = 1$) predicted by the free molecular flow equations.[12]

Shown in Fig. 8b, the dimensionless number flux to the afterbody surface of the wedge also relies on the leading-edge thickness. For a sharp wedge, $t/\lambda_\infty = 0.0$ ($Kn_t = \infty$); the dimensionless number flux is low at the leading edge and increases substantially up to a maximum value at about $1.0\lambda_\infty$ from the leading edge. A similar behavior is seen for slightly flat-faced leading edges, $t/\lambda_\infty \leq 0.1$ ($Kn_t \geq 10$). In contrast, for the bluntest leading-edge case investigated, $t/\lambda_\infty = 1.0$ ($Kn_t = 1$), the dimensionless number flux is large at the shoulder and decreases gradually along the body surface. The possible reason for this increase in the dimensionless number flux with increasing the leading-edge thickness can be related to the collisions of two groups of molecules, the molecules reflecting from the body and the molecules oncoming from the freestream. The molecules that are reflected from the body surface, which have a lower kinetic energy, interact with the oncoming freestream molecules, which have a higher kinetic energy. Thus, the surface-reflected molecules recollide with the body surface, which produce an increase in the dimensionless number flux in this region.

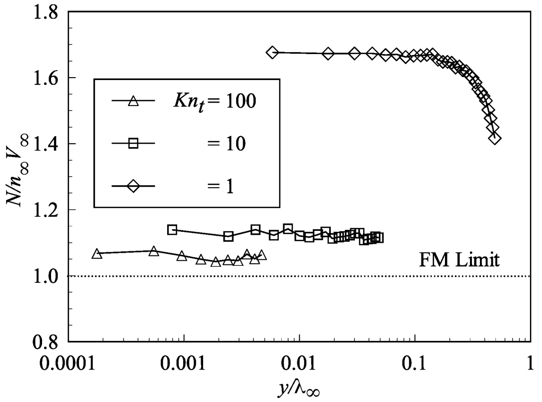

a) Front surface

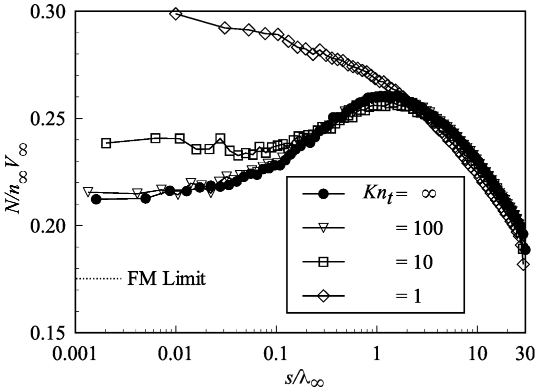

b) Wedge surface

Fig. 8 Dimensionless number flux along the front and wedge surfaces as a function of the Knudsen number Kn_t.

Referring to Fig. 8b, one can see that the downstream influence of the leading-edge thickness on the dimensionless number flux is approximately the order of the thickness t. By comparing to the free molecular limit, the dimensionless number fluxes to the afterbody surface of the wedges are well above that value predicted by free molecular flow.

The pressure p_w on the wedge surface is calculated by the sum of the normal momentum fluxes of both incident and reflected molecules at each time step. A flux is regarded as positive if it is directed toward the surface. Results are presented in terms of the pressure coefficient C_p.

The effects of the leading-edge thickness on the pressure coefficient obtained by DSMC method are illustrated in Fig. 9. Figure 9a displays the pressure coefficient on the front surface as a function of the dimensionless height y/λ_∞, and Fig. 9b illustrates the pressure coefficient along the afterbody surface of the wedge as a function of the dimensionless length s/λ_∞.

Referring to Fig. 9a, it can be seen that the pressure coefficient is basically constant along the front surface and increases with increasing Knudsen number Kn_t, for the $t/\lambda_\infty < 1.0$ cases. For the $t/\lambda_\infty = 1.0$ case, the pressure coefficient increases slightly in the vicinity of the shoulder. As the number of molecules impinging on the front surface decreases in the vicinity of the shoulder (see Fig. 8), then the normal component of the thermal velocity of the molecules increases as the flow approaches the shoulder of the leading edge.

The general shape of the pressure coefficient along the afterbody surface is similar to that presented by the number flux, that is, the pressure coefficient increases in the vicinity of the shoulder with falling Knudsen number Kn_t.

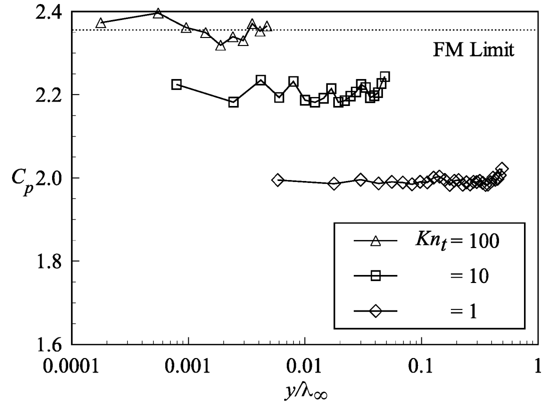

a) Front surface

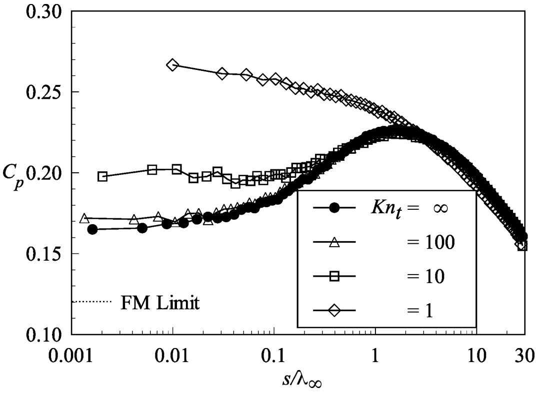

b) Wedge surface

Fig. 9 Pressure coefficient along the front and wedge surfaces of the wedge as a function of the Knudsen number Kn_t.

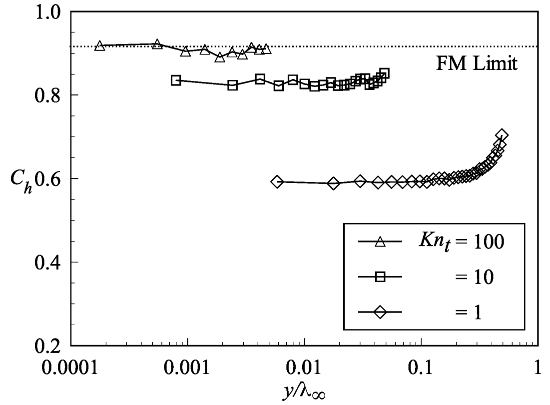

a) Front surface

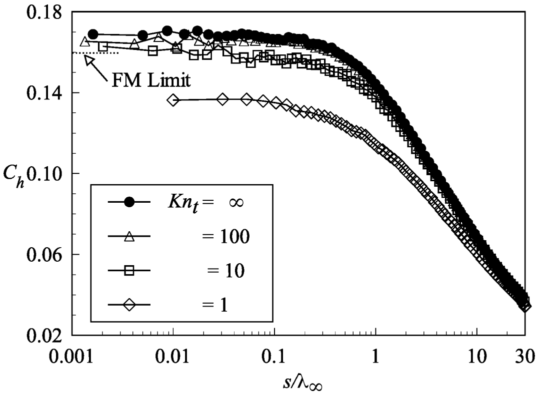

b) Wedge surface

Fig. 10 Heat-transfer coefficient along the front and wedge surfaces as a function of the Knudsen number Kn_t.

Plotted along with the computational solutions for pressure coefficient is the pressure coefficient predicted by the free molecular flow. As a reference, the free molecular flow values for pressure coefficient on front surface and along the afterbody surface are 2.35 and 0.12, respectively. Therefore, for the thinnest flat-faced leading edge investigated, $t/\lambda_\infty = 0.01$, the flow approaches the free collision flow in the vicinity of the stagnation point (Fig. 9a), as was pointed out earlier. Nevertheless, according to Fig. 9b, the flow is far from free collision value for the leading-edge thicknesses investigated, even though for the sharp wedge case, $t/\lambda_\infty = 0.0$.

The heat flux q_w to the wedge surface is calculated by the net energy fluxes of the molecules impinging on the surface. The net heat flux is related to the sum of the translational, rotational, and vibrational energies of both incident and reflected molecules. The heat flux is normalized by $\rho_\infty V_\infty^3/2$ and presented in terms of heat-transfer coefficient C_h.

The heat flux to the body surface was defined in terms of the incident and reflected flow properties and based on the gas-surface interaction model of fully accommodated, complete diffuse reemission. The diffuse model assumes that the molecules are reflected equally in all directions, quite independently of their incident speed and direction. Because of the diffuse reflection model, the reflected thermal velocity of the molecules impinging on the surface is obtained from a Maxwellian distribution that takes into account the temperature of the body surface. In this fashion, as the wall temperature is the same for all the cases investigated, the number of molecules impinging on the surface plays the important role on the reflected contribution to the net heat flux to the body surface.

The leading-edge thickness effect on heat-transfer coefficient is demonstrated in Figs. 10a and 10b for the front and the afterbody surfaces, respectively. For purpose of comparison, Fig. 10 displays the heat-transfer coefficient predicted by the free molecular flow. It is seen from Fig. 10a that the heat-transfer coefficient is also sensitive to the leading-edge thickness. As would be expected, the blunter the leading edge the lower the heat-transfer coefficient along the front surface. For the bluntest case investigated, $t/\lambda_\infty = 1.0$ ($Kn_t = 1$), the heat-transfer coefficient increases in the vicinity of the shoulder. Based on the earlier behavior for pressure coefficient, this behavior would be expected because the thermal velocity of the molecules increases in the vicinity of the shoulder on the front surface. Furthermore, the contribution of the translational energy to the net heat flux varies with the square of the thermal velocity of the molecules.

According to Fig. 10b, the effect of leading-edge flat nose is to decrease the heat-transfer coefficient on the afterbody surface in the region near the shoulder of the wedges, as compared to the sharp wedge case.

The shear stress τ_w on the body surface is calculated by averaging the tangential momentum transfer of the molecules impinging on the surface. For the diffuse reflection model imposed for the gas-surface interaction, reflected molecules have a tangential moment equal to zero because the molecules essentially lose, on average, their tangential velocity component.

Results for shear stress are normalized by $\rho_\infty V_\infty^2/2$ and presented in terms of the dimensionless skin-friction coefficient C_f. The influence of the leading-edge thickness on the skin-friction coefficient obtained by DSMC method is displayed in Fig. 11, parameterized by the Knudsen number Kn_t. Figure 11a illustrates the skin-friction coefficient on the front surface, and Fig. 11b depicts the skin-friction coefficient along the afterbody surface.

According to Fig. 11a, the skin-friction coefficient is zero at the stagnation point and increases along the front surface up to the shoulder of the wedge because the tangent momentum of the molecules is increasing as the molecule velocity increases. Because the number of molecules impinging on the front surface decreases in the vicinity of the shoulder, as shown in Fig. 8a.

The general shape of the skin-friction coefficient on the afterbody surface of the wedge is similar to that for the heat flux. Another interesting feature in the skin-friction coefficient is that it is roughly

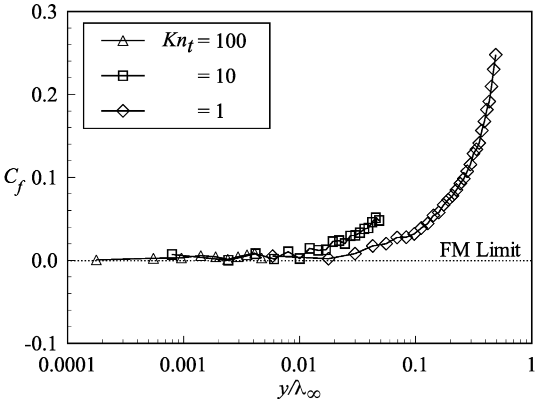

a) Front surface

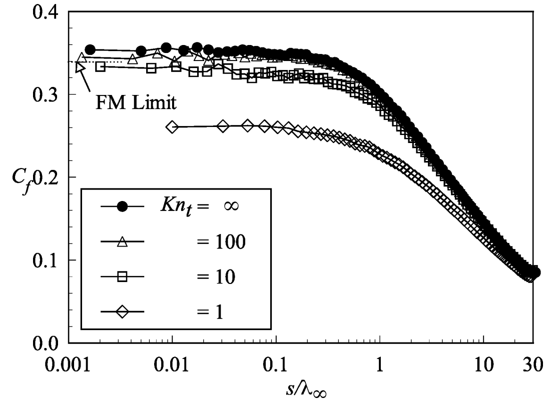

b) Wedge surface

Fig. 11 Skin-friction coefficient along the front and wedge surfaces as a function of the Knudsen number Kn_t.

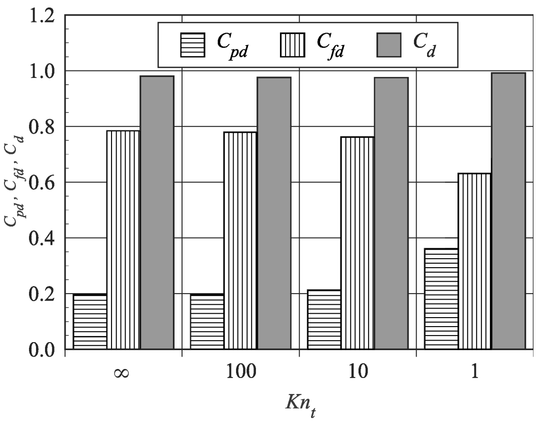

Fig. 12 Pressure drag, skin-friction drag, and total drag coefficients as a function of the Knudsen number Kn_t.

the same order of magnitude on both surfaces, in contrast to the pressure and heat transfer coefficients.

The drag on a surface in a gas flow results from the interchange of momentum between the surface and the molecules colliding with the surface. The total drag is obtained by the integration of the pressure p_w and shear stress τ_w distributions from the stagnation point of the leading edge to the station L that corresponds to the tangent point common to all the wedges (see Fig. 1). The values for the total drag were obtained by assuming the shapes acting as leading edges. Therefore, no base pressure effects were taken into account on the calculations. The DSMC results for total drag are normalized by $\rho_\infty V_\infty^2 H/2$ and presented as total drag coefficient C_d and its components of pressure drag coefficient C_{pd} and the skin-friction drag coefficient C_{fd}.

The extent of the changes in the drag coefficient C_d with increasing the leading-edge thickness is demonstrated in Fig. 12. It is seen that as the leading edge becomes flatter the contribution of the pressure drag increases and the contribution of the skin-friction drag decreases. As the net effect on total drag coefficient depends on these opposite behaviors, no appreciable changes are observed in the total drag coefficient for the leading-edge thicknesses investigated, except for the $Kn_t = 1$ case where total drag is slightly greater.

Comparison of Results

In this section, the DSMC results for pressure acting on and heat transfer to the wedge surface are compared to the available experimental data. The experimental data of Vidal and Bartz[3,5] used two flat-plate models, one small and the other large, in experimental wedge research. The wedge flows were produced by pitching the models to various compression angles. The small-scale flat plate model was designed to investigate the heat transfer in the vicinity of the leading edge, whereas the large-scale model was designed to investigate the wall pressure. The leading-edge model was flat faced with a thickness estimated to be 1.27×10^{-4} m (0.005 in.).

Figure 13 shows a comparison of the pressure on the wedge surface. In the figure, the vertical axis is the surface pressure normalized by the Newton–Buseman approximation for wedge pressure, and the abscissa is the normalized distance used by Vidal and Bartz.[5] The quantity C_* is the modified Chapman–Rubesin constant, which is defined by

$$C_* = (\mu_*/\mu_\infty)(T_\infty/T_*) \tag{1}$$

where μ_* is the viscosity at a reference temperature T_* given by

$$T_*/T_0 = \tfrac{1}{6} + \tfrac{1}{2}(T_w/T_0) \tag{2}$$

For comparison purpose, the surface pressure obtained from the theory of Chow and Eilers[23] is also shown in Fig. 13.

Referring to Fig. 13, the experimental data of Vidal and Bartz[5] are for wedges with half-angle of 10 deg, freestream Mach numbers of 19 (square symbols) and 20.7 (circle symbols), which correspond to freestream unit Reynolds numbers of 1.1×10^4/m and 8.5×10^4/m, respectively. It is seen from Fig. 13 that the DSMC results tend to the experimental data far from the nose of the leading edge, where the bluntness effects are no longer important. The surface measurements presented by Vidal and Bartz,[5] supposed to cover the transition from the strong interaction boundary-layer regime to the limit case of a free molecular flow, did not predict the pressure closer to the shoulder of the wedge when compared to the DSMC results. They expected that the surface pressure would approach to the free-molecular limit in the immediate vicinity of the leading edge. The difficulty arises from the complication of installing pressure taps very close to the nose of the leading edge. Furthermore, in low-density flows the true pressure on a surface can be significantly different from that measured in orifice cavities or pressure holes because of the increase in the effect of molecule-surface collisions, the

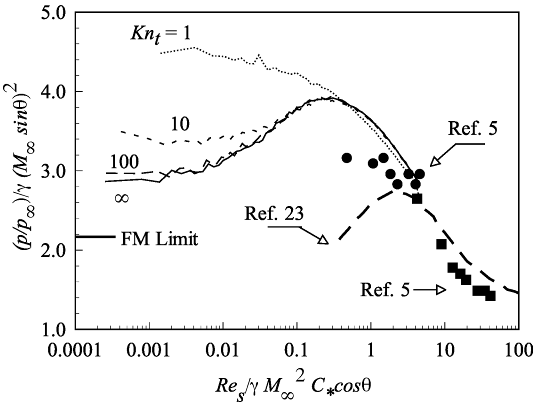

Fig. 13 Comparison of surface pressure along the wedge surface: ■ and ●, freestream Mach numbers of 19 and 20.7, respectively.

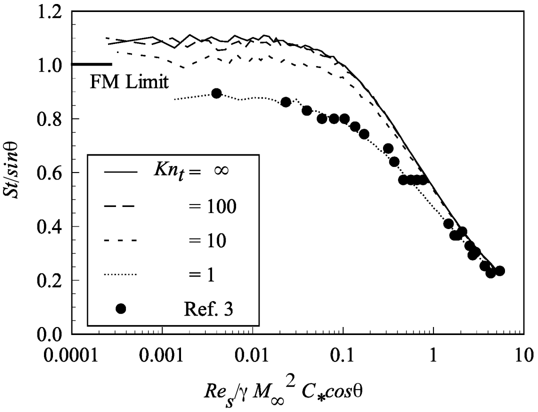

Fig. 14 Comparison of heat transfer along the wedge surface.

so-called orifice effect.[24] In addition, experimental measurements in the low-density conditions must detect extremely low pressure that require special instrumentation.

Figure 14 presents the comparison for the heat transfer to the wedge surface. In the figure, Stanton number St as a function of the Reynolds number Re is plotted. It can be seen the DSMC results for the heat flux follow the same trend shown by the experimental data. Nevertheless, despite the good agreement of the DSMC results for the $t/\lambda_\infty = 1.0$ case, which corresponds to $Kn_t = 1.0$, and that the experimental data were obtained for a wedge with a leading-edge thickness of 1.27×10^{-4} m (0.005 in.), no further conclusion can be drawn because it was not possible to identify the freestream conditions related to this leading-edge thickness as well as to calculate the mean free path from the various freestream conditions used by Vidal and Bartz.[3,5]

Conclusions

Through the use of DSMC method, the flow structure and the aerodynamic surface quantities about sharp and flat-faced wedges have been investigated. The calculations provided information concerning the nature of the flow in the vicinity of the nose resulting from variations in the leading-edge thickness for the idealized situation of two-dimensional hypersonic rarefied flow. The results are important to quantitatively define the flow physics of various leading-edge sizes at hypersonic speed and to aid in the design of future airbreathing leading-edge applications.

As expected, performance results for leading-edge thicknesses corresponding to Kn_t of ∞, 100, 10, and 1 indicated that the flow approaches free molecular flow in the vicinity of the front surface of the wedge as the leading-edge thickness decreases, for the flow conditions considered. It was observed that even though for a slightly flat-faced leading edge, thickness of one-hundredth of the freestream mean free path, the flow structure was affected far from the nose of the leading edge, when compared to the freestream mean free path.

Substantial changes in the surface quantities were observed as the leading-edge thickness increased. Number flux and pressure coefficient increased in a region the order of the leading-edge thickness downstream of the flat-faced shoulder. In addition, the heat-transfer coefficient and the skin-friction coefficient decreased and affected a larger region downstream of the shoulder.

References

[1] Nonweiler, T. R. F., "Aerodynamic Problems of Manned Space Vehicles," *Journal of the Royal Aeronautical Society*, Vol. 63, Sept. 1959, pp. 521–528.

[2] Cheng, H. K., Hall, J. G., Golian, T. C., and Hertzberg, A., "Boundary-Layer Displacement and Leading-Edge Bluntness Effects in High-Temperature Hypersonic Flow," *Journal of the Aerospace Sciences*, Vol. 28, No. 5, 1961, pp. 353–381.

[3] Vidal, R. J., and Bartz, J. A., "Experimental Studies of Low-Density Effects in Hypersonic Wedge Flows," *Rarefied Gas Dynamics*, edited by J. H. de Leeuw, Vol. I, Academic Press, New York, 1966, pp. 467–486.

[4] McCroskey, W. J., Bogdonoff, S. M., and Genchi, A. P., "Leading Edge Flow Studies of Sharp Bodies in Rarefied Hypersonic Flow," *Rarefied Gas Dynamics*, edited by C. L. Brundin, Academic Press, New York, 1967, pp. 1047–1066.

[5] Vidal, R. J., and Bartz, J. A.,"Surface Measurements on Sharp Flat Plates and Wedges in Low-Density Hypersonic Flow," *AIAA Journal*, Vol. 7, No. 6, 1969, pp. 1099–1109.

[6] Allgre, J., Herpe, G., and Faulmann, D., "Measurements of Pressure Distribution, Drag and Lift on Flat Plates and Wedges at Mach 8 in Rarefied Gas Flow," *Proceedings of the 6th International Symposium on Rarefied Gas Dynamics*, edited by L. Trilling and H. Y. Wachman, Vol. I, Academic Press, New York, 1969, pp. 465–482.

[7] Klemm, F. J., and Giddens, D. P., "A Numerical Solution to the Problem of Low-Density Hypersonic Wedge Flow," *Rarefied Gas Dynamics*, edited by J. L. Potter, Vol. 51, Pt. 1, Progress in Astronautics and Aeronautics, AIAA, New York, 1977, pp. 313–322.

[8] Anderson, J. L., "Tethered Aerothermodynamic Research for Hypersonic Waveriders," *Proceedings of the 1st International Hypersonic Waverider Symposium*, Univ. of Maryland, College Park, MD, 1990.

[9] Potter, J. L., and Rockaway, J. K., "Aerodynamic Optimization for Hypersonic Flight at Very High Altitudes," *Rarefied Gas Dynamics: Space Sciences and Engineering*, edited by B. D. Shizgal and D. P. Weaver, Vol. 160, Pt. 1, Progress in Astronautics and Aeronautics, AIAA, Washington, DC, 1994, pp. 296–307.

[10] Rault, D. F. G., "Aerodynamic Characteristics of a Hypersonic Viscous Optimized Waverider at High Altitude," *Journal of Spacecraft and Rockets*, Vol. 31, No. 5, 1994, pp. 719–727.

[11] Graves, R. E., and Argrow, B. M., "Aerodynamic Performance of an Osculating-Cones Waverider at High Altitudes," AIAA Paper 2001-2960, June 2001.

[12] Bird, G. A., *Molecular Gas Dynamics and the Direct Simulation of Gas Flows*, Oxford Univ. Press, Oxford, 1994.

[13] Garcia, A. L., and Wagner, W., "Time Step Truncation Error in Direct Simulation Monte Carlo," *Physics of Fluids*, Vol. 12, No. 10, 2000, pp. 2621–2633.

[14] Bird, G. A., "Monte Carlo Simulation in an Engineering Context," *Rarefied Gas Dynamics*, edited by Sam S. Fisher, Vol. 74, Pt. 1, Progress in Astronautics and Aeronautics, AIAA, New York, 1981, pp. 239–255.

[15] Borgnakke, C., and Larsen, P. S., "Statistical Collision Model for Monte Carlo Simulation of Polyatomic Gas Mixture," *Journal of Computational Physics*, Vol. 18, No. 4, 1975, pp. 405–420.

[16] Alexander, F. J., Garcia, A. L., and Alder, B. J., "Cell Size Dependence of Transport Coefficient in Stochastic Particle Algorithms," *Physics of Fluids*, Vol. 10, No. 6, 1998, pp. 1540–1542.

[17] Alexander, F. J., Garcia, A. L., and Alder, B. J., "Erratum: Cell Size Dependence of Transport Coefficient Is Stochastic Particle Algorithms," *Physics of Fluids*, Vol. 12, No. 3, 2000, p. 731.

[18] Hadjiconstantinou, N. G., "Analysis of Discretization in the Direct Simulation Monte Carlo," *Physics of Fluids*, Vol. 12, No. 10, 2000, pp. 2634–2638.

[19] Haas, B. L., and Fallavollita, M. A., "Flow Resolution and Domain Influence in Rarefied Hypersonic Blunt-Body Flows," *Journal of Thermophysics and Heat Transfer*, Vol. 8, No. 4, 1994, pp. 751–757.

[20] Bertin, J. J., *Hypersonic Aerothermodynamics*, AIAA Education Series, AIAA, Washington, DC, 1994, pp. 22–31.

[21] Gupta, R. N., Scott, C. D., and Moss, J. N., "Slip-Boundary Equations for Multicomponent Nonequilibrium Airflow," NASA TP-2452, Nov. 1985.

[22] Liepmann, H. W., Narasimha, R., and Chahine, M., "Theoretical and Experimental Aspects of the Shock Structure Problem," *Proceedings of the 11th International Congress of Applied Mechanics*, edited by H. Gortler, 1964, pp. 973–979.

[23] Chow, W. L., and Eilers, R. E., "Hypersonic Low-Density Flow past Slender Wedges," *AIAA Journal*, Vol. 6, No. 1, 1968, pp. 177–179.

[24] Potter, J. L., Kinslow, M., and Boylan, D. E., "An Influence of the Orifice on Measured Pressures in Rarefied Flow," *Rarefied Gas Dynamics*, edited by J. H. de Leeuw, Vol. 2, Academic Press, New York, 1966, pp. 175–194.

A. Ketsdever
Associate Editor